Detection of Periodic Forced Oscillations in Power Systems Incorporating Harmonic Information

Urmila Agrawal, *Student Member, IEEE*, and John W. Pierre, *Fellow, IEEE*

***Abstract*—This paper derives an improved version of a periodogram detector for detecting forced oscillations (FOs) in power systems using synchrophasor measurements. FOs are usually periodic in nature and are often accompanied with multiple harmonic components. This harmonic information of FOs is incorporated into the proposed periodogram detector, which significantly improves its detection performance for a given probability of a false alarm. The original periodogram detector carries out detection of each component of FOs separately, even though they are related through their harmonics. In the proposed periodogram detector, the detection algorithm is re-derived by incorporating harmonic information such that the detector now looks for a combination of harmonic components of FOs for detection. This derivation shows a significant improvement in the detection performance of the proposed periodogram detector as compared to the original one. This is also illustrated by the results obtained by implementing the proposed periodogram detector on the simulated and real-world PMU measurements.**

***Index Terms*—Forced oscillations (FOs), detection, periodic signal, phasor measurement unit (PMU), signal processing, periodogram, statistical analysis.**

I. Introduction

OSCILLATIONS in power systems play a significant role in maintaining reliable power systems operations. These oscillations often contain critical information on the operating conditions of a system, such as small-signal stability margin, which can help system operators take timely action to ensure system's uninterrupted operations. The availability of time-synchronized measurements by phasor measurement units (PMU) have led to the development of a large number of algorithms to study these oscillations in greater detail [1]–[5]. Depending on the nature of their origin, these oscillations can be broadly classified into electromechanical and forced oscillations (FO). Where the electromechanical oscillations are inherent to a system and arise from interactions among electrical and mechanical components of the system, FOs are the result of some rogue input driving the system. Some of the sources of FOs are malfunctioning control valves, stable limit cycles induced by a Hopf bifurcation in the hard control limiters, etc. as described in [6], [7]. These oscillations have some undesirable effects such as reducing power transfer limits, which can be of a concern when the system has already reached a stress-point, or damaging system equipments. Also, FOs can bias the system mode estimates, obtained from mode-meter algorithms, giving inaccurate information on the system small-signal stability margin [3]. A number of large FO examples are presented in [8]. Various algorithms have been developed to deal with these challenges posed by the presence of FOs as described in [9]. Paper [4], [10], [11] and references therein propose methods for the source localization of FOs so that some corrective action, as described in [1], can be taken to eliminate these oscillations. Paper [2] have proposed a method for accurately estimating system modes in the presence of FOs. However, all these algorithms first require that the presence of FOs in the system be detected.

Some methods to detect FOs are described in [5], [12]. Paper [12] utilizes the coherence spectrum between a signal and a delayed version of the same signal to detect sustained oscillations, which can include both FOs and undamped electromechanical oscillations. The threshold for detecting forced oscillation using this coherence method is developed in [13] and the method to estimate the coherence spectrum is presented in [14]. The method proposed in [5] is a modified version of the periodogram detector described in [15] that is designed to work with FOs embedded in the white ambient noise. The modified periodogram detector is re-formulated to work with FOs embedded in the colored ambient noise that is suited for power systems applications. This detector considers each component of FOs individually even though they are related through their harmonics, and hence the detection of these components of FOs is carried out separately from each other. As a result, this detector does not give the best detection performance when the FO present in the signal consists of multiple harmonic components. Analysis of real-world PMU measurements has shown that FOs are often accompanied with multiple harmonic components [5].

In this paper, a new version of a periodogram detector is derived that incorporates the harmonic information of FOs, such that the proposed detector now looks for a combination of fundamental and harmonic components of FOs for detection of FOs. This helps detect one or more harmonic components, including fundamental, of FOs that are smaller in amplitude and would have otherwise remained undetected by the original periodogram detector. This paper includes a detailed theoretical statistical analysis of the proposed detector to analyze its detection performance. This theoretical analysis shows an improvement

Manuscript received April 13, 2018; revised June 20, 2018; accepted July 21, 2018. Date of publication July 24, 2018; date of current version December 19, 2018. This work was supported by the University of Wyoming Engineering Initiative and DOE under Contracts DE-SC0012671 and DE-AC02-05CH11231. Paper no. TPWRS-00546-2018. *(Corresponding author: Urmila Agrawal.)*

The authors are with the Department of Electrical and Computer Engineering, University of Wyoming, Laramie, WY 82071 USA (e-mail: uagrawal@uwyo.edu; pierre@uwyo.edu).

Color versions of one or more of the figures in this paper are available online at http://ieeexplore.ieee.org.

Digital Object Identifier 10.1109/TPWRS.2018.2859301

in the probability of detection for a given probability of a false alarm. As small-signal electromechanical oscillations are not accompanied with harmonic components, detecting a combination of components of FOs can also help distinguish between critically damped electromechanical oscillations and FOs [1], which is another advantage of the proposed detector.

The rest of the paper is organized as follows. Section II discusses the background theory required for the derivation of the proposed periodogram detector. Proposed method is derived in Section III and its effectiveness is validated in Section IV using simulated and real-world data for different cases. Section V concludes the paper.

II. Background Theory

This section briefly discusses the signal model representing PMU measurements that consist of FOs embedded in the ambient noise and some of the statistical definitions that will be required for development of the proposed detector.

A. Signal Model

The PMU measurements consisting of FOs and the ambient noise are modeled as

$$y[n] = w[n] + s[n], \tag{1}$$

where n is the discrete time index, $w[n]$ is the response of the system to the random load variations that continuously drive the system referred to as ambient noise and $s[n]$ is the deterministic periodic FOs given by

$$s[n] = \sum_{i=1}^{L} A_i cos\left(i\omega_o n + \Phi_i\right), \tag{2}$$

where ω_o is the frequency of the fundamental component of the FO in radians/sample, L is the number of harmonic components and A_i and Φ_i are the amplitude and the phase of the i^{th} harmonic component of the FO.

B. Statistical Definitions

A number of statistical terms are used in the derivation of the proposed periodogram detector. Some of the important ones are described below:

- Hypothesis-testing [16]
  Hypothesis testing is a method of testing a claim or hypothesis about some characteristics of data if it belongs to a certain group or not. For the FO detection problem, the hypothesis testing determines if an FO is present in the signal or not. The hypothesis that the signal does not contain an FO is the null-hypothesis and that the signal contains an FO is the alternative-hypothesis.
- Probability of a false alarm and detection [16]
  In hypothesis testing problems, there are two types of error. The first type of error, referred to as a false alarm, occurs when the null hypothesis is rejected under null hypothesis, which means that the detector detects an FO in the presence of ambient noise only. The probability with which this occurs is called the probability of a false alarm. The second type of error, referred to as a miss, occurs when the alternative hypothesis is rejected under alternative hypothesis, which means that the detector misses to detect the presence of an FO. The probability with which the second type of error occurs is called the probability of a miss. The probability of detection, which gives the probability by which a FO is accurately detected, is obtained by subtracting the probability of a miss from one.
- Test-statistic and detection-threshold [17]
  Test-statistic is a function of the data, under analysis, calculated to determine which of the two hypothesis, null and alternate, is to be rejected. The detection threshold is calculated using the probability distribution function (pdf) of the test-statistic under null-hypothesis. If the test-statistic exceeds the detection threshold, then the null-hypothesis is rejected i.e. an FO is detected for this detection problem.

III. Proposed Method

In this paper, a new version of a periodogram detector is developed by incorporating harmonic information of the FOs into the detector. For this, mathematical formulation for the test-statistic and its statistical properties, detection threshold and the probability of a detection are derived with harmonic information incorporated in the detection algorithm. For practical applications, the harmonic components of the FOs actually present in a signal are not known. Thus, different combinations of harmonic components are chosen and the detection process is carried out for these combinations of the harmonic components so as to detect harmonic components actually present in the signal. A detection threshold is calculated for each of the combinations and then the test statistic is compared with each of the detection thresholds separately. FOs are detected only if the test-statistic exceeds the threshold for a combination of frequency bins corresponding to all harmonic components selected in that step. The detection results obtained for all considered combinations of harmonic components are then combined such that the final detection result is given by the union of the detection results obtained in each step.

A. Test-Statistic and Its Statistical Properties

The periodogram is a standard test-statistic used for detecting the presence of sinusoids in a signal, also used in [15], and given by

$$\hat{\phi}(\omega_k) = \frac{1}{N}\left|\sum_{n=1}^{N} y(n)e^{-i\omega_k n}\right|^2, \tag{3}$$

where N is the number of samples in the data analysis window and ω_k is the frequency in radians/sample given by

$$\omega_k = \frac{2\pi k}{N^z}, \quad 0 \le k \le \frac{N^z}{2}, \tag{4}$$

where N^z is the zero-padded length of the periodogram such that $N^z \ge N$. When an FO is present in a signal, the periodogram of the signal consists of sharp peaks at the frequencies of the FOs. However, these sharp peaks can also be caused by statistical fluctuations [15]. Thus, some threshold is required that can help

distinguish a peak representing a component of FOs from that caused by statistical fluctuations, such that an FO is detected only if the peak values of the periodogram exceed the thresholds [15] at the frequencies of the components of FOs. This detection threshold is obtained by using the pdf of the scaled periodogram, also referred to as the scaled test-statistic, given by

$$\hat{\phi}'_T(\omega_k) = \frac{2\hat{\phi}(\omega_k)}{\phi_w(\omega_k)}, \tag{5}$$

where $\hat{\phi}(\omega_k)$ is the periodogram of the signal, which is the test-statistic, and $\phi_w(\omega_k)$ is the true ambient noise spectrum and gives power of the ambient noise at the k^{th} frequency bin.

As derived in [15] for the white noise case and modified in [5] assuming the noise spectrum to be colored and known, the scaled periodogram of a signal containing only ambient noise follows a central chi-squared distribution given by

$$\hat{\phi}'_T(\omega_k) \sim \chi^2_2, \tag{6}$$

where χ^2_2 symbolizes a chi-squared distribution with 2 degrees of freedom and '$\sim$' is read as *is distributed as*. When only ambient noise is present, the scaled periodogram have identical and independent distribution [5], [15]. Similarly, the scaled test-statistic for a signal consisting of an FO, given by (2), embedded in the ambient noise follows a non-central chi-squared distribution given by

$$\hat{\phi}'_T(i\omega_o) \sim {\chi'_2}^2(\lambda_i) \text{ for } i = 1, 2, ..., L, \tag{7}$$

where ${\chi'_2}^2(\lambda_i)$ symbolizes a non-central chi squared distribution with 2 degrees of freedom and the non-central parameter, λ_i, given by

$$\lambda_i = \frac{dA_i^2}{2\phi_w(i\omega_o)} = OSNR_i \tag{8}$$

for the i^{th} component of the FO. Here d is the duration of the FO in the signal and $OSNR_i$ is the output signal to noise ratio calculated at the frequency of the i^{th} component of the FO [5], [15]. The $OSNR_i$, defined here, is different from the traditionally defined total signal to noise ratio (SNR) as $OSNR_i$ is calculated only using the component of the noise spectrum at the frequency of the i^{th} component of the FO and not a sum of the noise spectrum over all considered frequency bins. The detection performance of the periodogram detector is a function of the output SNR, as defined here, and not the total SNR.

B. Formulation of the Detection Threshold

The detection of the periodic signal, given by (2), embedded in the ambient noise is represented by the hypothesis testing problem [15] given by

$$\begin{aligned} H_0 &: y[n] = w[n] \text{ for } n = 1, 2, \ldots, N \\ H_1 &: y[n] = s[n] + w[n] \text{ for } n = N_1 + 1, \ldots, N_2 \text{ and} \\ &\quad = w[n] \text{ for } n = 1 \text{ to } N_1 \text{ and } n = N_2 + 1 \text{ to } N; \end{aligned} \tag{9}$$

where the FO is present from $N_1 + 1$ to N_2 such that the FO duration is $d = N_2 - N_1$, H_0 is the null hypothesis rejecting the presence of the FO and H_1 is the alternative hypothesis rejecting the absence of the FO [15]. In detection problems, the detection threshold, γ, is calculated using the probability of a false alarm, which is a user-specified variable and selected as a trade-off between the probability of occurrence of a false alarm and the probability of detection [15]. The smaller the value of the probability of a false alarm, the higher will be the detection threshold and hence, smaller will be the probability of detection. Usually, the probability of a false alarm is selected in the range of 10^{-3} to 10^{-8}. Mathematically, the probability of a false alarm is given by

$$P_{fa} = P(\text{ saying } H_1 \text{ is true} | H_0 \text{ is true}),$$

where | is read as *given*. For the periodogram detector described in [5], a false alarm occurs when the test-statistic exceeds the detection threshold for any individual frequency bin. For the proposed detector, a false alarm occurs only when the test-statistic exceeds the threshold for a combination of frequency bins corresponding to the selected combination of harmonic components. For example, if the harmonic components selected are $[\,1 \quad 3 \quad 5\,]$, a false alarm occurs when the test-statistics exceed the thresholds for a combination of frequencies related by these harmonic components.

Let's assume, we are taking into consideration harmonic components given by $\mathbf{K}$ such that

$$\mathbf{K} = [\,K_1 \quad K_2 \quad \cdots \quad K_M\,],$$

where K's correspond to the harmonic numbers of interest. For the first step, $\mathbf{K} = [1]$, which looks for each component of FOs individually for detection and also corresponds to the periodogram detector described in [5]. For the second and the following steps, any combination of harmonic components can be selected, for example $\mathbf{K} = [\,1 \quad 3\,]$ for the first and the third harmonics, and so on. As already explained, a false alarm occurs when the test-statistic for each of the M selected harmonic components exceed thresholds for at least one fundamental frequency bin i.e. $\hat{\phi}(K_m\omega_o) > \gamma(K_m\omega_o)$ for $m = 1, \ldots, M$ for at least one value of $\omega_o \,\epsilon\, \Omega$, where Ω is the set of frequencies for which the periodogram is calculated. Then, the probability of a false alarm is given by

$$\begin{aligned} P_{fa} &= P\left(\bigcup_{i=1}^{\frac{N_B}{K_M}} \left\{ \bigcap_{m=1}^{M} \left(\hat{\phi}(K_m\omega_i) > \gamma(K_m\omega_i)\right)\right\} \middle| H_0\right) \\ &= 1 - P\left(\bigcup_{i=1}^{\frac{N_B}{K_M}} \left\{ \bigcap_{m=1}^{M} \left(\hat{\phi}(K_m\omega_i) > \gamma(K_m\omega_i)\right)\right\} \middle| H_0\right)^c, \end{aligned} \tag{10}$$

where N_B is the total number of frequency bins considered for the detection purpose, 'c' denotes complement, ω_i is the frequency corresponding to the i^{th} frequency bin. As the harmonic components are incorporated, i ranges from 1 to N_B/K_M only, instead of N_B such that $(K_M\omega_i)$ will range upto N_B. Here, N_B is a user-specified variable selected on the basis of the frequency range of interest for detection and can range upto the folding frequency. As N_B increases, the probabillity of a false

alarm also increases. Using DeMorgan's law [17], (10) can be written as

$$P_{fa} = 1 - P\left(\bigcap_{i=1}^{\frac{N_B}{K_M}} \left\{ \bigcup_{m=1}^{M} \left(\hat{\phi}(K_m\omega_i) \leq \gamma(K_m\omega_i)\right)\right\} \middle| H_0\right)$$

$$= 1 - P\left(\bigcap_{i=1}^{\frac{N_B}{K_M}} \left\{ \bigcup_{m=1}^{M} \left(\frac{2\hat{\phi}(K_m\omega_i)}{\phi_w(K_m\omega_i)} \leq \frac{2\gamma(K_m\omega_i)}{\phi_w(K_m\omega_i)}\right)\right\} \middle| H_0\right). \tag{11}$$

As described earlier, the distribution of the scaled periodogram for different frequency bins are independent under null hypothesis. However, distribution of the union of the scaled periodograms for different values of i are not independent as they can share common frequency bins. For mathematical tractability, it is assumed that the distribution of the union of the scaled periodograms are independent for different values of i resulting in an upper bound on the probability of a false alarm given by,

$$P_{fa} \leq 1 - \prod_{i=1}^{\frac{N_B}{K_M}} P\left(\bigcup_{m=1}^{M} \left(\frac{2\hat{\phi}(K_m\omega_i)}{\phi_w(K_m\omega_i)} \leq \frac{2\gamma(K_m\omega_i)}{\phi_w(K_m\omega_i)}\right) \middle| H_0\right) \tag{12}$$

as $P(A \bigcap B) \geq P(A).P(B)$ and equality sign holds when A and B are independent. Now, the detection threshold is chosen to be a scaled version of the true ambient noise spectrum i.e. $\gamma(\omega) = \gamma' \times \phi_w(\omega)/2$, where γ' is the scaled detection threshold corresponding to the scaled test-statistic given by $\hat{\phi}'_T(\omega)$. This assumption is valid as the threshold for detecting FOs should be a function of the ambient spectrum such that threshold for frequency bins having a higher ambient spectral content should have a higher threshold while detecting FOs and vice-versa. Thus, (12) becomes

$$P_{fa} \leq 1 - \prod_{i=1}^{\frac{N_B}{K_M}} P\left(\bigcup_{m=1}^{M} \left(\hat{\phi}'_T(K_m\omega_i) \leq \gamma'\right) \middle| H_0\right). \tag{13}$$

Again, using DeMorgan's law, we have

$$P_{fa} \leq 1 - \prod_{i=1}^{\frac{N_B}{K_M}} \left\{1 - P\left(\bigcup_{m=1}^{M} \left(\hat{\phi}'_T(K_m\omega_i) \leq \gamma'\right) \middle| H_0\right)^c\right\}$$

$$= 1 - \prod_{i=1}^{\frac{N_B}{K_M}} \left\{1 - P\left(\bigcap_{m=1}^{M} \left(\hat{\phi}'_T(K_m\omega_i) > \gamma'\right) \middle| H_0\right)\right\}. \tag{14}$$

As the distribution of the scaled test-statistic for different frequency bins are independent, we have

$$P_{fa} \leq 1 - \prod_{i=1}^{\frac{N_B}{K_M}} \left\{1 - \prod_{m=1}^{M} P\left(\hat{\phi}'_T(K_m\omega_i) > \gamma' | H_0\right)\right\}. \tag{15}$$

The cumulative distribution function of the scaled test-statistic, $\hat{\phi}'_T(K_m i)$, is given by

$$P\left(\hat{\phi}'_T(K_m\omega_i) \leq \gamma' | H_0\right) = 1 - e^{-\gamma'/2}$$

$$P\left(\hat{\phi}'_T(K_m\omega_i) > \gamma' | H_0\right) = e^{-\gamma'/2}$$

for a central chi-squared distribution with 2 degrees of freedom [17]. Thus, (15) becomes

$$P_{fa} \leq 1 - \prod_{i=1}^{\frac{N_B}{K_M}} \left(1 - \prod_{m=1}^{M} e^{-\gamma'/2}\right)$$

$$= 1 - \prod_{i=1}^{\frac{N_B}{K_M}} \left(1 - e^{-\gamma' M/2}\right)$$

$$= 1 - \left(1 - e^{-\gamma' M/2}\right)^{\frac{N_B}{K_M}}. \tag{16}$$

To calculate the detection threshold, we only consider the maximum probability of false alarm, $P_{fa,max}$, i.e. the worst case scenario. Using the argument that for a small $P_{fa,max}$, $e^{-\gamma' M/2} << 1$, we have $(1 - e^{-\gamma' M/2})^{\frac{N_B}{K_M}} \approx 1 - \frac{N_B}{K_M} e^{-\gamma' M/2}$ [15]. Thus, (16) becomes

$$P_{fa,max} = \frac{N_B}{K_M} e^{-\gamma' M/2}. \tag{17}$$

Rearranging equation (17) in terms of $P_{fa,max}$, we have

$$\gamma' = -\frac{2}{M} ln\left(\frac{K_M}{N_B} P_{fa,max}\right), \tag{18}$$

which gives the detection threshold corresponding to the scaled test statistic, given by (7). The detection threshold for the test-statistic, given by the periodogram, is then given by

$$\gamma(\omega) = -\frac{\phi_w(\omega)}{M} ln\left(\frac{K_M}{N_B} P_{fa,max}\right)$$

$$= \frac{\phi_w(\omega)}{M}\left(ln\left(\frac{N_B}{K_M}\right) + ln\left(\frac{1}{P_{fa,max}}\right)\right). \tag{19}$$

As expected, the detection threshold for the proposed detector is directly proportional to the ambient noise spectrum. The detection threshold is inversely proportional to the number of harmonic components selected, M. As the number of harmonic components increases, the detection threshold decreases for a given maximum probability of a false alarm and thereby the probability of detection increases. The detection threshold is also directly proportional to the sum of the natural logarithm of the number of frequency bins, given by $\frac{K_M}{N_B}$, for which the detector looks for the fundamental component and the natural logarithm of the maximum probability of a false alarm. As seen from this expression, the detection threshold may not always be dominated by the maximum probability of a false alarm and will depend on the number of frequency bins. However, for the case when the inverse of the maximum probability of a false alarm is significantly higher than the number of frequency bins for which the detector looks for the fundamental component,

the detection threshold will be proportional to the natural log of the inverse of the maximum probability of a false alarm, and the number of frequency bins will not have much effect on the detection threshold.

So far, zero-padding while calculating periodogram of the signal has not been included in the formulation of the probability of a false alarm. When a signal is zero-padded for calculating the periodogram of the signal, the distribution of the scaled test-statistic for nearby frequency bins are no longer independent. However assuming frequency bins to be independent corresponds to the worst-case scenario, and anything else would not increase the maximum probability of a false alarm. Thus, (18) and (19) holds true even for the case when the signal is zero-padded while calculating the periodogram of the signal, however N_B would then correspond to the number of frequency bins after zero-padding operation.

C. Formulation of the Probability of a Detection

For each combination of harmonics considered, an FO is detected only when the test-statistic exceeds the threshold for all the harmonic components. The probability of a detection, P_d, is obtained by using the distribution of the scaled test-statistic under the alternative hypothesis, given by (7), and the detection threshold, given by (19), as follows,

$$\begin{aligned} P_d &= P(\text{saying } H_1 \text{ is true} | H_1 \text{ is true}) \\ &= P(\hat{\phi}'_T(K_1\omega_o) > \gamma' \cap \cdots \cap \hat{\phi}'_T(K_M\omega_o) > \gamma' | H_1) \\ &= P\left(\bigcap_{i=1}^{M} \left(\hat{\phi}'_T(K_i\omega_o) > \gamma'\right) \middle| H_1\right). \end{aligned} \tag{20}$$

Using DeMorgan's law, (20) becomes

$$P_d = 1 - P\left(\bigcup_{i=1}^{M} \left(\hat{\phi}'_T(K_i\omega_o) \leq \gamma'\right) \middle| H_1\right). \tag{21}$$

Now, we define K_{min} such that

$$K_{min} = \arg\min_{K_i} \hat{\phi}'_T(K_i\omega_o) \quad \forall i = 1, 2, \ldots M,$$

which corresponds to the harmonic component for which the scaled test-statistic has the minimum value. Let ω_{min} be the frequency corresponding to the K_{min} and A_{min} be the amplitude of the K_{min}^{th} harmonic component of the FO. If $\hat{\phi}'_T(K_{min}\omega_o)$ is less than the scaled detection threshold, then the alternative hypothesis will be rejected no matter what the value of the scaled test-statistic is for other harmonic components. Thus using (18), (21) can be written as

$$\begin{aligned} P_d &= 1 - P\left(\hat{\phi}'_T(K_{min}\omega_o) \leq \gamma' | H_1\right) \\ &= Q_{\chi'^2_2(\lambda_{K_{min}})}(\gamma'), \end{aligned} \tag{22}$$

where Q represents the complementary cumulative distribution function [17]. Here, Q, for a non-central chi-squared distribution, increases monotonically with the increase in the non-central parameter, given by (8) for $i = K_{min}$, which is given by the OSNR of the component of FOs having the minimum scaled test-statistic value. Also, Q decreases monotonically with the increase in γ'. Thus, the probability of a detection increases with an increase in the OSNR of the K_{min}^{th} component of the FO given by $\lambda_{K_{min}}$, which is a trait of the signal and cannot be controlled, and with a decrease in the detection threshold, which can be achieved by incorporating the harmonic information of FOs for a given maximum probability of a false alarm. This substantiates the claim of improvement in the detection performance by incorporating the harmonic information.

TABLE I
VALIDATION OF $P_{fa,max}$

$P_{fa,max}$	Estimated P_{fa}				
	K=[1]	K=[1 2]	K=[1 3]	K=[1 2 4]	K=[1 3 5]
0.001	0.0015	0.0013	0.0009	0.0008	0.0007
0.005	0.0057	0.0068	0.0046	0.0028	0.0029
0.01	0.0107	0.0126	0.0107	0.0049	0.0048

IV. RESULTS AND DISCUSSIONS

The performance of the proposed detector was analyzed and compared with the periodogram detector described in [5] using both simulated data and real-world data. Simulated data helped analyze the statistical performance of the algorithms by running Monte-Carlo trials, random quantity being the unique set of random load variarions that excites the system, and real-world measured data helped understand the practical applicability of the proposed detector for real-time operations. In addition to analyzing the detection performance, simulated data were also used to validate the expression derived for the maximum probability of a false alarm given by (17). Simulated data were generated using the minniWECC model [18], and real-world data were from the Eastern-Interconnection (EI) recorded in 2007. Frequency measurements, obtained by taking time derivative of the voltage angle measurements, were used for both simulated and real-world data.

A. Results Using Simulated Data

The minniWECC model is a reduced order dynamic model of the WECC system, the details of which can be found in [18]. This model uses actual system values, and hence closely mimics the real system. Forced input is represented by a modulation signal added to the mechanical power input to the source generator. The true ambient noise spectrum was calculated using the state-space matrices of the minniWECC model for implementing the proposed detector.

The first set of results validates the theoretical expression derived for the maximum probability of a false alarm given by (17). Different values of the maximum probability of a false alarm and combination of the harmonic components were considered as shown in Table I. 20,000 Monte-Carlo trials were run using 10 minutes of ambient noise for each case. Fig. 1 shows the signal for one of the trials. Frequency range of interest was chosen from 0.1 Hz to 1 Hz. Table I shows the results obtained for different cases and as seen, the estimated probability of a

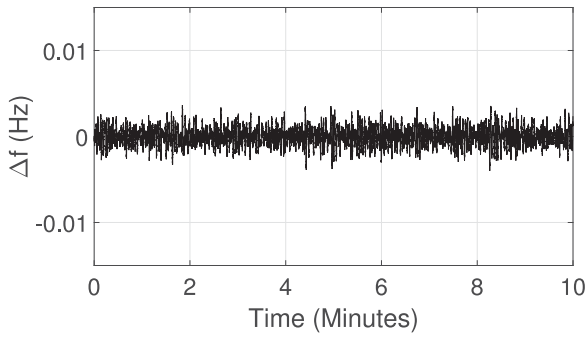

Fig. 1. Signal containing ambient noise only.

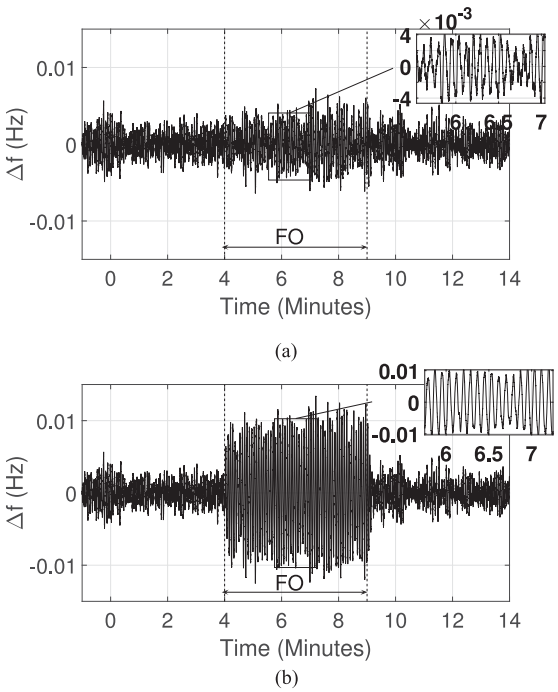

Fig. 2. Signal for one of the trials for each of the cases. (a) $OSNR_1 = 23$ dB. (b) $OSNR_1 = 33$ dB.

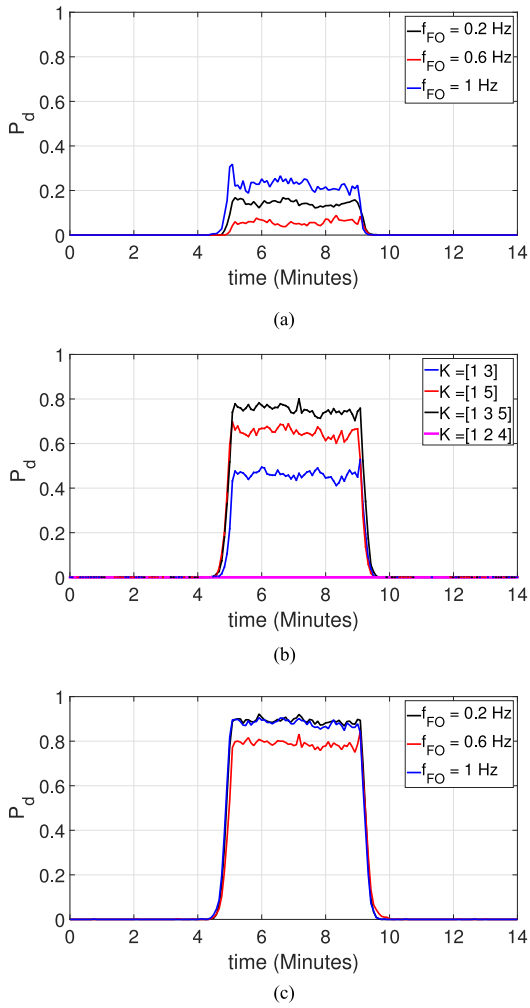

Fig. 3. Detection results for FOs with $OSNR_1 = 23$ dB and $P_{fa,max} = 10^{-7}$. (a) Different component of FOs for K = [1]. (b) Different combinations of **K**. (c) Final detection result.

false alarm was close to the theoretical maximum probability of a false alarm thereby validating the derived expression.

The second set of results analyzes the detection performance of the proposed detector based on 500 Monte-Carlo trials. The forced input was obtained by taking a sum of three sinusoidal signals having frequencies of 0.2, 0.6 and 1 Hz such that the FO contained odd harmonic components only. Two different cases were considered based on the amplitude of the FO. For the first case, a mid-sized FOs having an OSNR of 23 dB (total SNR $= -1.25$ dB) calculated at the frequency of the fundamental component of the FO was considered. As the OSNR was calculated using the component of the ambient noise spectrum only at the fundamental frequency of the FO, OSNR of 23 dB resulted in a small amplitude FO slightly visible in the time domain, as seen in Fig. 2(a) containing FOs from $t = 4$ to 9 minutes. For the second case, a high-amplitude FO having an OSNR of 33 dB (total SNR $= 8.75$ dB), shown in Fig. 2(b), was considered. The maximum probability of a false alarm was equal to 10^{-7}. A detection sliding window of 1 minute was used to get each detection result and the data window was updated every 5 seconds. The results shown for data window at $t = 0$ used signal from $t = -1$ to $t = 0$ minute and the data analysis window contained FOs from $t = 4$ to 10 minutes. The different combination of harmonic components selected were $\{1, [1\ \ 2], [1\ \ 3], [1\ \ 4], [1\ \ 5], [1\ \ 2\ \ 3], [1\ \ 2\ \ 4]\}$ and $\{[1\ \ 3\ \ 5]\}$.

Fig. 3(a)–3(c) show the detection results for the proposed periodogram detector for different value of **K** obtained over 500 Monte-Carlo trials for the first case with $OSNR_1 = 23$ dB. Fig. 3(a) shows the estimated probability of detection of different components of the FO for $\mathbf{K} = 1$ that carries out detection of each component of FOs individually. As seen, the performance of the periodogram detector was poor for all components of the FO for $\mathbf{K} = 1$. The estimated probability of detection of the fundamental and the harmonic components were significantly improved by incorporating the harmonic components $\mathbf{K} = [1\ 3]$ and [1 5], and further improved for $\mathbf{K} = [1\ 3\ 5]$ as seen in Fig. 3(b), where the fundamental component corresponds to

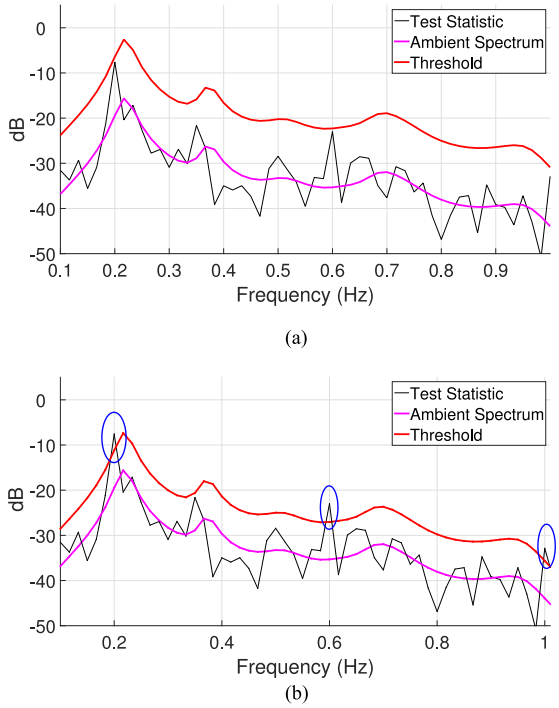

Fig. 4. Illustration of the proposed detector for $OSNR_1 = 23$ dB and $P_{fa,max} = 10^{-7}$. (a) $\mathbf{K} = [1]$. (b) $\mathbf{K} = [1\ 3\ 5]$.

0.2 Hz FO component. As the FO contained odd harmonic components only, the estimated probability of detection was zero for $\mathbf{K} = [1\ 2]$, [1 4], [1 2 3] and [1 2 4], as illustrated in Fig. 3(b) for $\mathbf{K} = [1\ 2\ 4]$. The final detection result was obtained by combining the results obtained for all considered combinations of harmonic components. From the final detection result for different component of FOs, shown in Fig. 3(c), it can be seen that the periodogram detector gives much better performance by incorporating harmonic information.

The change in the behavior of the periodogram detector by incorporating harmonic information is illustrated using Fig. 4(a) and Fig. 4(b) for one of the trials for the data analysis window at $t = 8.5$ minute. Here, the ambient spectrum, detection threshold and the test-statistic are shown in dB scale for a better analysis, and the component of the FO detected in each step is enclosed by a blue-colored ellipse. Fig. 4(a) corresponds to $\mathbf{K} = 1$ for which no component of the FO was detected. With the harmonic information incorporated for $\mathbf{K} = [1\ 3\ 5]$, the detection threshold decreased and the fundamental and the considered harmonic component of the FOs were detected as seen in Fig. 4(b).

Results for the second case with FOs having an $OSNR_1$ of 33 dB are shown in Fig. 5(a)–5(c). Here, the detector performed well for the fundamental component of the FO for K = 1. However, the performance was poor for other components of FOs. By incorporating the harmonic information, the proposed detector performed well for all the components of the FOs as seen in Fig. 5(c). This is also illustrated using Fig. 6(a) and 6(b) for one of the trials for the data analysis window at t = 8.5 minutes, which shows an improvement in the performance of the detector by incorporating harmonic information of the FOs. Here, even though the detection performance of the periodogram detector

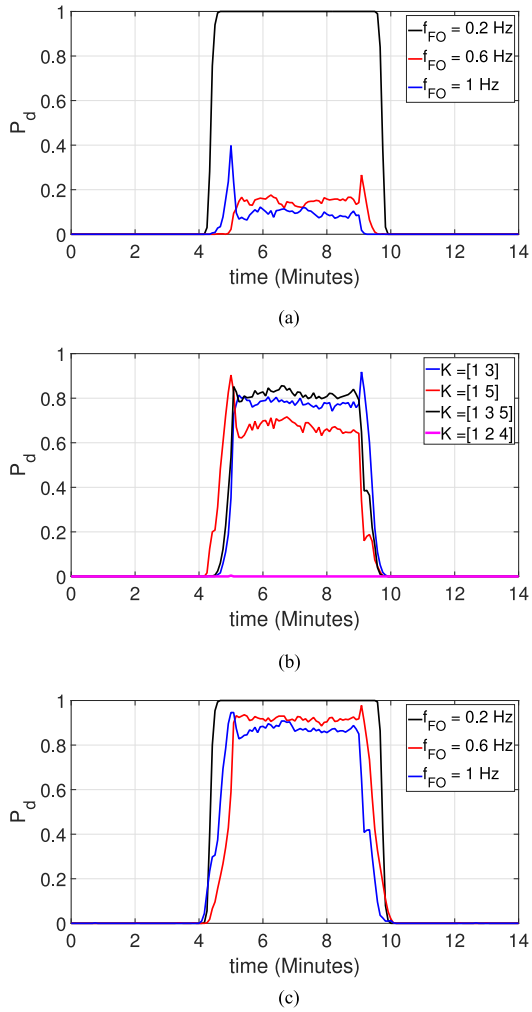

Fig. 5. Detection results for FOs with $OSNR_1 = 33$ dB and $P_{fa,max} = 10^{-7}$. (a) Different component of FOs for K=[1]. (b) Different combinations of **K**. (c) Final detection result.

for the fundamental component did not show any improvement by incorporating harmonic information, the detection of the harmonic components can help power systems operators ascertain that the sustained oscillation present in a signal is in-fact a forced oscillation and not a lightly damped natural oscillation.

The computational complexity of the proposed detector was also analyzed to examine its applicability for real-time operations. The algorithm was implemented on a Dell-Precision T1650 desktop having a 64-bit Intel(R) Core(TM)i7-6700 @ 3.41 GHz processor and 32 GB of RAM. The average algorithm implementation time for a single trial, based on 500 trials, ranged from 0.0032 sec, for the case when no FO was detected, to 0.0047 second when FOs were detected. Thus, the proposed detector is well-suited for real-time applications.

B. Result Using PMU Measurements

The proposed detector was implemented on the real-world measured data, shown in Fig. 7, collected from the Eastern-Interconnection (EI) in 2007. Due to the confidentiality requirement, only the year and the system from where the

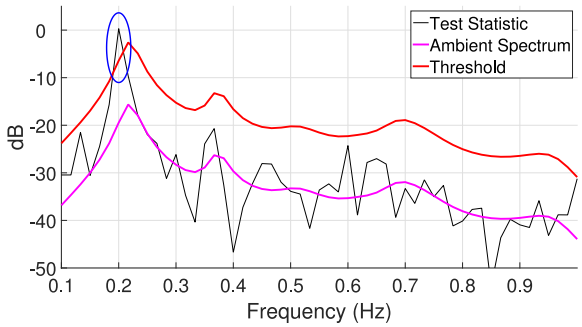

(a)

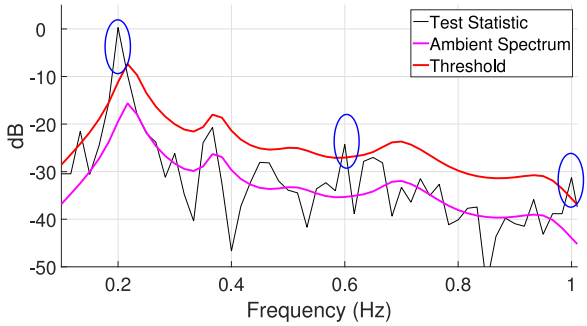

(b)

Fig. 6. Illustration of the proposed detector for $OSNR_1 = 33$ dB and $P_{fa,max} = 10^{-7}$. (a) $\mathbf{K} = [1]$. (b) $\mathbf{K} = [1\ 3\ 5]$.

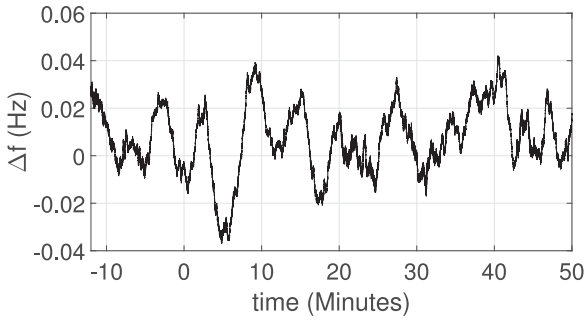

Fig. 7. Real-world measured data from EI.

measurements were collected are mentioned. The real-world data can contain missing data or outliers. For this, the corrupt data, such as outliers, were removed, and the removed and the missing data were replaced by new interpolated data, which is a common approach to dealing with short periods of missing and corrupt data. The ambient noise spectrum required for implementing the periodogram detector was obtained using the method described in [19]. The maximum probability of a false alarm was set to 10^{-4}. The combination of harmonic components selected were same as that used for obtaining results with the simulated data. Since the FO in the signal was very small and persistent throughout the data, a data block of 12 minutes was used here to obtain results and the data window was updated every 15 seconds. The results obtained at $t = 0$ minutes uses signal from $t = -12$ to 0 minutes and so on.

Fig. 8(a)-8(b) show the detection results obtained for $\mathbf{K} = 1$ and $\mathbf{K} = [1\ 2]$ respectively over a time-period of 50 minutes.

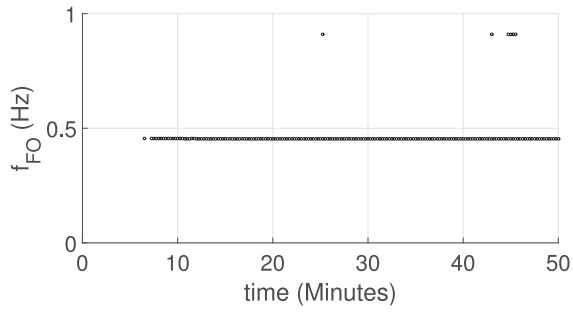

(a)

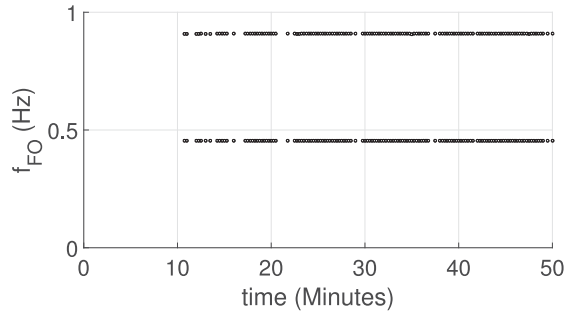

(b)

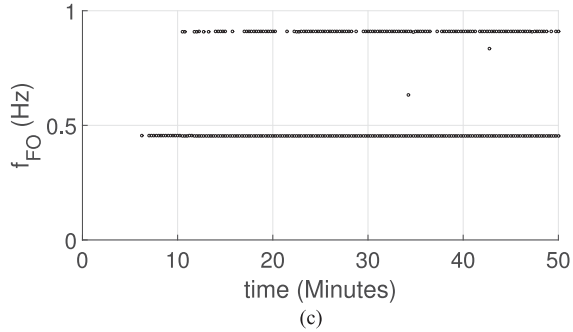

(c)

Fig. 8. Detection results for EI data. (a) Detection result for $\mathbf{K} = [1]$. (b) Detection result for $\mathbf{K} = [1\ 2]$. (c) Final detection result.

The other combinations did not detect any FOs and so the results for these combinations are not included. From the final detection result shown in Fig. 8(c), it can be seen that the FO present in the signal contained second harmonic component at 0.909 Hz in addition to the fundamental component at 0.455 Hz. The second harmonic component was detected by only a few data analysis window for $\mathbf{K} = 1$ and thus it could have been mistaken as a false alarm. As the frequency of the FO was close to that of a system mode having frequency of around 0.49 Hz, it could also have given a false impression of the decrease in the damping ratio of a system mode. However, when incorporating the harmonic information, the second harmonic component was detected consistently ascertaining that the oscillation was in-fact a forced response of the system. These results show an improvement in the performance of the periodogram detector by incorporating harmonic information and validates the ability of the proposed detector to distinguish between electromechanical and forced oscillations based on the presence of harmonic components. The methodology of the proposed detector is illustrated in Fig. 9 for data analysis window at $t = 13$ minute.

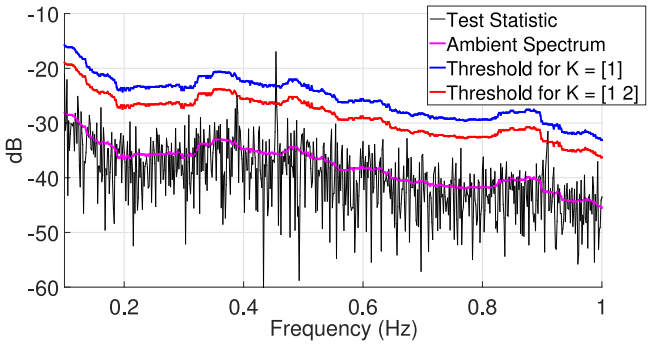

Fig. 9. Illustration of the proposed detector using EI data.

V. Conclusion

The results obtained using the simulated and the real measured data show a significant improvement in the detection performance of the proposed periodogram detector by incorporating harmonic information of the FOs. The proposed detector can detect different combination of harmonic components, for example odd only harmonic components as illustrated by results obtained using simulated data, and even only harmonic components as illustrated by results obtained using real-world data. The results obtained using real measured data also highlights another advantage of the proposed detector of its capability to distinguish between the sustained electromechanical and forced oscillations by detecting a combination of the multiple components of FO. As the component of the FOs at higher frequency range (typically greater than 1 Hz) usually have the highest amplitude at the measurement location closest to the source, the proposed detector can also help in locating the source of FOs by detecting the component of the FOs at higher frequency range. This will be a focus of the future work. The performance of the proposed detector can be further improved by including other aspects of the detector such as windowing and zero-padding of the signal, using multiple detection segments, etc described in [5]. Overall, the proposed periodogram detector can be used as an improved tool for real-time applications for simultaneously detecting a combination of multiple components of FOs.

Acknowledgment

The authors would like to thank J. Follum from the Pacific Northwest National Laboratory for valuable discussions, D. Trudnowski from Montana Tech for providing code for the minniWECC model, and the Power System Research Consortium for EI synchrophasor data.

References

[1] R. Xie and D. Trudnowski, "Distinguishing features of natural and forced oscillations," in *Proc. IEEE Power Energy Soc. General Meeting*, 2015, pp. 1–5.
[2] J. Follum, J. Pierre, and R. Martin, "Simultaneous estimation of electromechanical modes and forced oscillations," *IEEE Trans. Power Syst.*, vol. 32, no. 5, pp. 3958–3967, Sep. 2017.
[3] L. Vanfretti, S. Bengtsson, V. S. Perić, and J. O. Gjerde, "Effects of forced oscillations in power system damping estimation," in *Proc. IEEE Int. Workshop Appl. Meas. Power Syst.*, 2012, pp. 1–6.
[4] U. Agrawal, J. W. Pierre, J. Follum, D. Duan, D. Trudnowski, and M. Donnelly, "Locating the source of forced oscillations using PMU measurements and system model information," in *Proc. IEEE Power Energy Soc. General Meeting*, 2017, pp. 1–5.
[5] J. Follum and J. W. Pierre, "Detection of periodic forced oscillations in power systems," *IEEE Trans. Power Syst.*, vol. 31, no. 3, pp. 2423–2433, May 2016.
[6] P. B. Reddy and I. A. Hiskens, "Limit-induced stable limit cycles in power systems," in *Proc. IEEE Russia Power Tech*, 2005, pp. 1–5.
[7] Y.-h. Xu, R. He, and Z. Han, "The cause analysis of turbine power disturbance inducing power system low frequency oscillation of resonance mechanism," in *Proc. Chin. Soc. Elect. Eng.*, vol. 27, no. 17, 2007, pp. 83–87.
[8] D. Kosterev *et al.*, "Implementaiton and operation experience with oscillation detection application at Bonneville Power Administration," in *Proc. CIGRE Grid Future Symp.*, 2016, pp. 1–5.
[9] M. Ghorbaniparvar, "Survey on forced oscillations in power system," *J. Modern Power Syst. Clean Energy*, vol. 5, no. 5, pp. 671–682, 2017.
[10] F. Ghorbaniparvar and H. Sangrody, "PMU application for locating the source of forced oscillations in smart grids," in *Proc. IEEE Power Energy Conf. Illinois*, 2018, pp. 1–5.
[11] N. Zhou, M. Ghorbaniparvar, and S. Akhlaghi, "Locating sources of forced oscillations using transfer functions," in *Proc. IEEE Power Energy Conf. Illinois*, 2017, pp. 1–8.
[12] N. Zhou and J. Dagle, "Initial results in using a self-coherence method for detecting sustained oscillations," *IEEE Trans. Power Syst*, vol. 30, no. 1, pp. 522–530, Jan. 2015.
[13] M. Ghorbaniparvar and N. Zhou, "Bootstrap-based hypothesis test for detecting sustained oscillations," in *Proc. Power Energy Soc. General Meeting*, 2015, pp. 1–5.
[14] M. Ghorbaniparvar, N. Zhou, and X. Li, "Coherence function estimation with a derivative constraint for power grid oscillation detection," in *Proc. IEEE Global Conf. Signal Inf. Process.*, 2016, pp. 791–795.
[15] S. M. Kay, *Fundamentals of Statistical Signal Processing: Detection Theory*, vol. 2. Upper Saddle River, NJ, USA: Prentice-Hall, 1998.
[16] F. J. Gravetter and L. B. Wallnau, *Statistics for the Behavioral Sciences*. Boston, MA, USA: Cengage Learning, 2016.
[17] G. Casella and R. L. Berger, *Statistical Inference*, vol. 2. Pacific Grove, CA, USA: Duxbury, 2002.
[18] D. Trudnowski, "The MinniWECC system model—Appendix 2 of J. Undrill and D. Trudnowski, Oscillation Damping Controls," Bonneville Power Administration Portland, OR, USA, Year 1 report 37508, Sep. 2008.
[19] J. Follum, F. Tuffner, and U. Agrawal, "Applications of a new nonparametric estimator of ambient power system spectra for measurements containing forced oscillations," in *Proc. IEEE Power Energy Soc. General Meeting*, Jul. 2017, pp. 1–5.

Urmila Agrawal received the B.E. degree in electrical engineering from Pulchowk Campus, Kathmandu, Nepal, in 2011, the M.S. degree in electrical engineering and the Ph.D. degree in electrical engineering with a minor in statistics from the University of Wyoming, Laramie, WY, USA, in 2014 and 2018, respectively. She worked as an Electrical Design Engineer from 2011 to 2012 with Hulas Engineering & Construction Pvt. Ltd., Kathmandu. She worked as a Summer Intern with Pacific Northwest National Laboratory (PNNL), in 2016, where she is currently working as a Power Systems Engineer. Her research interests include the application of statistical signal processing techniques to solve challenging problems in power systems.

John W. Pierre (S'86–M'86–S'87–M'91–SM'99–F'13) received the B.S. degree in electrical engineering with a minor in economics from Montana State University, Bozeman, MT, USA, in 1986, and the M.S. degree in electrical engineering with a minor in statistics and the Ph.D. degree in electrical engineering from the University of Minnesota, Minneapolis, MN, USA, in 1989 and 1991, respectively. He worked as an Electrical Design Engineer at Tektronix before attending the University of Minnesota. In 1992, he joined the faculty,Electrical and Computer Engineering Department, University of Wyoming (UW), Laramie, WY, USA, where he is currently the G.J. Guthrie Nicholson Chaired Professor of power engineering. He served as an Interim Department Head from 2003 to 2004 and received UWs College of Engineering Graduate Teaching and Research Award in 2005. His research interests include statistical signal processing applied to power systems. Dr. Pierre is a member of the IEEE Signal Processing, Education, and Power & Energy Societies. In 2015, he received the Distinguished Graduate Mentor Award, which is a University wide award for outstanding mentorship of graduate students.